State Estimation based on the Concept of Continuous Symmetry and Observability Analysis: The Case of Calibration

Agostino Martinelli

State Estimation based on the Concept of Continuous Symmetry and Observability Analysis: The Case of Calibration

Agostino Martinelli

***Abstract*—This paper considers the problem of state estimation in autonomous navigation from a theoretical perspective. In particular, the investigation regards problems where the information provided by the sensor data is not sufficient to carry out the state estimation (i.e. the state is not observable). For these systems, the concept of continuous symmetry is introduced. Detecting the continuous symmetries of a given system has a very practical importance. It allows us to detect an observable state whose components are non linear functions of the original non observable state. So far this theoretical and very general concept has been applied to deal with two distinct fundamental estimation problems in the framework of mobile robotics. The former is in the framework of self-calibration and the latter is in the framework of the fusion of the data provided by inertial sensors and vision sensors. For reasons of length, only the former is discussed. In particular, the theoretical machinery is used to address a specific calibration problem. The solution constrains the robot to move along specific trajectories in order to be able to apply the calibration algorithm. This paper provides two distinct contributions. The first is the introduction of this concept of continuous symmetry. The second is the introduction of a simple and efficient strategy to extrinsically calibrate a bearing sensor (e.g. a vision sensor) mounted on a vehicle and, simultaneously estimate the parameters describing the systematic error of its odometry system. Many accurate simulations and real experiments show the robustness, the efficiency and the accuracy of the proposed strategy.**

***Index Terms*—State Estimation and Navigation, Observability, Sensor Fusion, Sensor Calibration.**

I. Introduction

Autonomous navigation often requires to solve different tasks simultaneously (e.g. localization, mapping, obstacle avoidance etc.). Among them, several are estimation tasks, i.e. the robot has to be able to autonomously estimate a given state by integrating the information contained in its sensor data. Typical examples of estimation problems fundamental in many robotics applications are localization, SLAM and self-calibration.

In every estimation problem the following fundamental questions must be answered:

1) Does the system contain the necessary information to perform the estimation of the considered state?
2) If not, is it possible to detect a new state which can be estimated? And, more importantly: what is the link between this new state and the data provided by the robot's sensors?

A. Martinelli is with INRIA Rhone Alpes, Montbonnot, France e-mail: agostino.martinelli@ieee.org

The answer to the first question is provided by a well known concept developed in the framework of control theory: the observability. In control theory, a system is defined observable when it is possible to reconstruct its initial state by knowing, in a given time interval, the system inputs and the outputs [8]. Commonly, in wheeled robotics the system inputs are the angular speeds of the wheels. They can significantly differ from the values of the controls delivered to the wheel actuators because of many noise sources. These inputs are evaluated by the robot proprioceptive sensors (typically wheel encoders). The outputs are evaluated by the exteroceptive sensors.

The observability properties can easily be derived in a linear system by performing the Kalman canonical decomposition (see, e.g., [8]). However, in a non linear system, this concept is much more complex and the observability becomes a local property [15]. In this case, the concept of *Weak Local Observability* was introduced by Hermann and Krener [15]. The word *weak* means that only the distinguishability of states which are "close" is taken into account[1]. In other words, if two points which are not close produce exactly the same inputs and outputs, the state is clearly not observable. But, it can still be weakly observable. For more details, the reader is addressed to [15]. The same authors also introduced a criterion, the *observability rank criterion*, to verify whether a system has this property. In particular, the two theorems 3.1 and 3.11 in [15] state that a system is *Weak Local Observable* (WLO) if and only if it satisfies the rank criterion[2]. The application of the rank criterion only requires to perform differentiation. In this paper we assume that a system contains the information to perform the estimation of the state if and only if the system is WLO. Obviously, in order to estimate a state, it is necessary that the system is WLO. However, the contrary cannot be true in some special situations. For instance, this assumption does not take into account the sensor noise. Furthermore, it can be wrong for the kidnapping problem since to solve this problem it is necessary to distinguish states which are in general not close. We believe that this assumption is true in many estimation problems within the framework of autonomous navigation. On the other hand, this assumption

[1]Two points can be defined close when any ball set centered on one of them also contains the other one.

[2]Actually, theorem 3.11 states that if the system is WLO, the observability rank condition is satisfied generically. We focus our attention to the word "generically" which means that there are cases where the system is WLO, but the rank condition is not satisfied. However, the probability of this event is very small. For more details we address the reader to [15].

has already been adopted in previous works which investigate several estimation problems in the context of mobile robotics (see section I-B). This assumption allows us to give an answer to the first question by simply performing differentiation.

Answering the second question is in general much harder, and could be done by using the theory of distributions [17]. When a system is not WLO anywhere, there are in general infinite initial states reproducing exactly the same inputs and outputs. Let us consider for instance, the $2D$ localization problem when the robot moves along a corridor, equipped with odometry sensors and sensors able to perform relative observations (e.g. bearing and range sensors). In this situation, all the initial states differing for a shift along the corridor, reproduce exactly the same inputs and outputs. Intuitively, we remark that the entire system has one continuous symmetry that corresponds with the shift along the corridor. It is obvious that the only quantities that we can estimate (i.e. which are WLO) are invariant with respect to this continuous symmetry (i.e. the robot orientation and the distance of the robot from the corridor walls). The previous consideration regarding this simple localization problem is quite trivial and it's not required to introduce special mathematical tools. However, there are cases where answering the second question is a very challenging task. The key to deal with these cases is to first provide a mathematical definition of continuous symmetry able to generalize the intuitive idea of symmetry.

In the theory of distributions introduced in [17], the concept of continuous symmetry is implicitly contained in the Frobenius theorem through the Lie brackets. In this paper, we provide a definition of continuous symmetry and from there, we derive a partial differential equation which must be satisfied by all the WLO quantities. The same partial differential equation is derived in [17]. However, the derivation here provided is much simpler since the Lie brackets, the Frobenius theorem and the concept of distribution do not need to be introduced. Therefore, it can be very useful for the mobile robotics community. Our definition of continuous symmetry is inspired by the concept of continuous symmetry adopted in theoretical physics [14]. Our definition allows us an immediate application of the concept of continuous symmetry to real cases. We then consider a fundamental calibration problem: the simultaneous self calibration of the odometry system and the extrinsic calibration of a bearing sensor. In particular, we consider the case when the calibration is carried out by only using a single point feature. To the best of our knowledge, this problem has never been investigated before. Contrary to the $2D$ localization in a corridor previously mentioned, it is impossible to derive the WLO quantities for this problem without performing analytical computation. We provide the steps to solve this calibration problem on the basis of the analytical results derived in the first part of this paper.

A. Related Works on Sensor Calibration in Mobile Robotics

In recent decades, the problem of sensor calibration has been considered with special emphasis in the field of computer vision. When a camera which has been previously calibrated (i.e. for which both the intrinsic and extrinsic parameters have been determined) is mounted on a robotics system, it is necessary to determine the new extrinsic parameters only. In the case of robot wrists, very successful approaches are based on the solution of a homogeneous transform equation of the form $AX = XB$ which is obtained by moving the robot wrist and observing the resulting motion of the camera [28], [32]. In particular, in the previous equation, A describes the configuration change of the wrist, B, the configuration change of the camera and X, the unknown camera configuration in the wrist reference frame. A and B are accurately known: A is obtained by using the encoder data and B by using the camera observations of a known object before and after the wrist movement [32]. In mobile robotics the situation changes dramatically and the previous methods cannot be applied. Unfortunately, the displacement of a mobile robot obtained by using the encoder data, is not as precise as in the case of a wrist. In other words, the previous matrix A is roughly estimated by the encoders. A possible solution to this inconvenience could be obtained by adopting other sensors to estimate the robot movement (i.e. the matrix A). However, most of the times, the objective is to estimate the camera configuration in the reference frame attached to the robot odometry system. Therefore, it is important to introduce a new method with the ability to simultaneously perform the extrinsic camera calibration and the calibration of the robot odometry system. So far, the two problems have been considered separately.

Regarding the odometry, a very successful strategy was introduced by Borenstein and Feng [7] in 1996 called the UMBmark method. It is based on absolute robot position measurements after the execution of several square trajectories. More recently, a method based on two successive least-squares estimations has been introduced [3]. Finally, very few approaches calibrate the odometry without the need of a priori knowledge of the environment and/or of the use of global position sensors (like a GPS) [12], [31], [34].

Regarding the problem of sensor to sensor calibration, several cases have recently been considered (e.g. IMU-camera [27], laser scanner-camera [9], [35], [36] and odometry-camera [24]).

B. Related Works on Observability Analysis in Mobile Robotics

Observability analysis has been carried out by several authors for the localization problem. Roumeliotis [30] applied this analysis to a multi-robot system. The analysis was performed through the linear approximation. The main result of this observability analysis was that the system is not observable and it becomes observable when at least one of the robots in the team has global positioning capabilities. Bonnifait and Garcia investigated the case of one robot equipped with encoders and sensors able to provide the bearing angles of known landmarks in the environment [6]. The observability analysis was carried out by linearizing the system (as in the previous case) and by applying the *observability rank condition*. As in many nonlinear systems, they found that in some cases, while the associated linearized system is not observable, the

system is WLO. Bicchi and collaborators extended the case of a single robot to the SLAM problem ([5], [20]). They studied one robot equipped with the same bearing sensors of the previous case. They considered landmarks in the environment with a priori known position and landmarks whose position had to be estimated. They found that two landmarks are both necessary and sufficient to make the system observable. They also applied optimal control methods in order to minimize the estimation error. In particular, in [20] they maximized the Cramer-Rao lower bound as defined in [18]. Very recently, the observability rank condition has been adopted to investigate the observability properties of the problem of calibrating a vision sensor [24] [27]. In addition, the observability rank criterion has recently been applied to the SLAM problem [16] [19]. Finally, an observability analysis was performed in order to investigate the properties of the concurrent bias estimation in the map aided localization problem [29].

However, throughout these studies the only thing determined is whether the state defining the system configuration is WLO or not.

C. Paper Contributions and Paper Structure

In this paper, we take an important step forward which is fundamental when dealing with a non observable problem. Indeed, when a state is not WLO, estimating the state directly brings inconsistencies with catastrophic consequences. On the other hand, when a state is not WLO, suitable functions of its components could be WLO and therefore could be estimated. We call these functions *Observable Modes*. The derivation of the observable modes is fundamental in order to properly perform the estimation.

We introduce some mathematical tools to derive the observable modes for systems which are not WLO. These mathematical tools are based on the concept of continuous symmetry which will be defined. This theoretical and very general concept has been applied to deal with two distinct fundamental estimation problems in the framework of mobile robotics. The former is in the framework of self-calibration, and the latter, is in the framework of the fusion of the data provided by inertial (IMU) and vision sensors. For reasons of length and the sake of simplicity, only the former is discussed. An exhaustive description and discussion about the latter can be found in [22] and [23].

This paper provides two distinct contributions:

- The introduction of the concept of continuous symmetry;
- The use of this concept to introduce a new strategy to robustly, efficiently and accurately estimate the parameters describing both the extrinsic bearing sensor calibration and the odometry calibration.

The second contribution was preliminary discussed in [25] and [26] where the same calibration problem was analyzed. In particular, in [25] a local decomposition for this system was performed in which, the robot accomplishes pure rotations and straight paths. In [26] the local decomposition was extended to all circular trajectory.

As it will be revealed, the application of the concept of continuous symmetry sometimes requires a big effort in terms of analytical computation. On the other hand, the computation has to be done only once and the solution provided is in general, simple.

Section II provides a very simple example to better illustrate the paper's first contribution. As for the previously mentioned $2D$ localization in a corridor, analytical methods are not required to detect the observable modes due to the simplicity of the chosen example. The theoretical concepts introduced in section III will be illustrated by referring to this example. In particular, we recall the rank criterion introduced by Hermann and Krener [15] and, we introduce the concept of continuous symmetry. Starting from this definition, we derive a partial differential equation which characterizes all the observable modes in a given system. In section IV we derive these observable modes for our calibration problem. Starting from the decomposition given in section IV, we introduce a very efficient strategy to perform the calibration in section V. Finally, we evaluate its performance in section VI, with simulations (VI-A) and experiments (VI-B). Conclusions are provided in section VII.

II. A Simple Example of Localization

We consider a mobile robot moving in a $2D$-environment. The configuration of the robot in a global reference frame, can be characterized through the vector $[x_R,\ y_R,\ \theta_R]^T$ where x_R and y_R are the cartesian robot coordinates, and θ_R is the robot orientation. The dynamics of this vector are described by the following non-linear differential equations:

$$\begin{cases} \dot{x}_R = v\cos\theta_R \\ \dot{y}_R = v\sin\theta_R \\ \dot{\theta}_R = \omega \end{cases} \tag{1}$$

where v and ω are the linear and the rotational robot speed respectively. The robot is equipped with proprioceptive sensors which are able to evaluate these two speeds. We assume that a point feature exists in our environment and, without loss of generality, we fix the global reference frame onto it (see figure $1a$). The robot is also equipped with a range sensor, able to evaluate the distance of the point feature. Therefore, our system has the following output:

$$y = D \equiv \sqrt{x_R^2 + y_R^2} \tag{2}$$

We also provide the equations for the same system in polar coordinates, i.e. when the robot configuration is described by the coordinates D, $\phi_R \equiv \arctan 2(y_R, x_R)$ and θ_R.

$$\begin{cases} \dot{D} &= v\cos(\theta_R - \phi_R) \\ \dot{\phi}_R &= \dfrac{v}{D}\sin(\theta_R - \phi_R) \\ \dot{\theta}_R &= \omega \\ y &= D \end{cases} \tag{3}$$

Our goal is to answer the two questions mentioned in the previous section for the system characterized by the equations (1-2) or (3). Since the system is very simple, we do not need special mathematical tools.

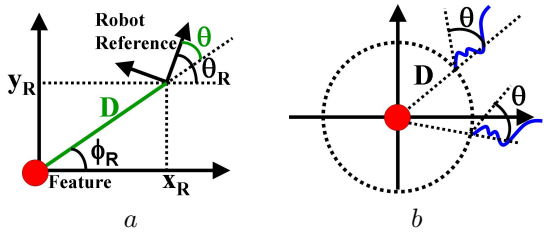

Fig. 1. A simple localization problem. The robot is equipped with odometry and range sensors able to evaluate the distance D (a). In b, the two trajectories are compatible with the same system inputs and outputs.

To check whether we have the necessary information to estimate the robot configuration $[x_R,\ y_R,\ \theta_R]^T$, we have to prove that it is possible to uniquely reconstruct the initial robot configuration by knowing the inputs and outputs (observations) in a given time interval. When at the initial time, the distance D from the origin is available, the estimated robot position belongs to a circumference (see figure $1b$). Furthermore, every orientation is possible. As soon as the robot moves accordingly with the inputs $v(t)$ and $\omega(t)$, it is possible to find one trajectory starting from each point on the circumference, providing the same distances from the origin by choosing a suitable initial robot orientation (e.g. in fig. $1b$ the two indicated trajectories provide the same distances from the origin at every time). Therefore, the dimension of the undistinguishable region is 1 and the dimension of the largest WLO subsystem is $3-1=2$.

We remark that the system has a continuous symmetry: the system inputs ($v(t)$ and $\omega(t)$), and outputs ($y(t)$), are invariant with respect to a rotation of the global frame about the vertical axis (in the next section we will provide a mathematical definition for a general continuous symmetry). Based on the fact that the dimension of the largest WLO subsystem is two, we know that we can only estimate two independent quantities. Furthermore, these two quantities must satisfy the previous system invariance, i.e. they must be rotation invariant. A possible choice is provided by the two quantities D and θ in figure 1.

$$\theta \equiv \theta_R - \arctan 2(y_R, x_R) \tag{4}$$

The new system is characterized by the following equations:

$$\begin{cases} \dot{D} = v\cos\theta \\ \dot{\theta} = \omega - \dfrac{v}{D}\sin\theta \\ y = D \end{cases} \tag{5}$$

which express the link between the new state $[D,\ \theta]^T$ and proprioceptive data ($v,\ \omega$) and the exteroceptive data (D).

The detection of the previous two observable modes and the derivation of the equations in (5) is fundamental (i.e the answer to the second question stated in the introduction). Indeed, estimating the original state brings inconsistencies with catastrophic consequences.

In the next section, we want to provide some mathematical tools (taken from control theory) in order to perform the same analysis. This will allow us to answer the two questions stated in the introduction, for more complicated estimation problems in the framework of autonomous navigation.

III. Continuous Symmetries and Observability Properties

A general characterization for systems in the framework of autonomous navigation, is provided by the following two equations, which describe the dynamics and the observation respectively:

$$\begin{cases} \dot{S} = f(S,u) = f_0(S) + \sum_{i=1}^{M} f_i(S)u_i \\ y = h(S) \end{cases} \tag{6}$$

where $S \in \Sigma \subseteq \Re^n$ is the state, $u = [u_1,\ u_2,\ ...,\ u_M]^T$ are the system inputs and $y \in \Re$ is the output (we are considering a scalar output for the sake of clarity; the extension to a multi dimensional output is straightforward). Both the systems defined by (1-2) or (3), and the one defined by (5), can be characterized by (6). For instance, for the system in (3), we have: $S = [D,\ \phi_R,\ \theta_R]^T$, $f_0 = [0,0,0]^T$, $M = 2$, $u_1 = v$, $u_2 = \omega$, $f_1(S) = [\cos(\theta_R - \phi_R),\ \frac{\sin(\theta_R-\phi_R)}{D},\ 0]^T$, $f_2(S) = [0,\ 0,\ 1]^T$, $h(S) = D$.

A. Observability Rank Criterion

We remind the reader of some concepts in the theory by Hermann and Krener in [15]. We will adopt the following notation: we indicate the k^{th} order Lie derivative of a field Λ, along the vector fields $v_{i_1}, v_{i_2}, ..., v_{i_k}$ with $L^k_{v_{i_1},v_{i_2},...,v_{i_K}}\Lambda$. The definition of the Lie derivative is provided by the following two equations:

$$L^0\Lambda = \Lambda,\ L^{k+1}_{v_{i_1},...,v_{i_{k+1}}}\Lambda = \nabla_S\left(L^k_{v_{i_1},...,v_{i_k}}\Lambda\right)\ .\ v_{i_{k+1}} \tag{7}$$

where the symbol "." denotes the scalar product. Now, let us refer to the system in (6), and let us indicate with Ω, the space of all the Lie derivatives $L^k_{f_{i_1},...,f_{i_k}}h$, $(i_1,...,i_k = 1,...,M)$ where the functions f_{i_j} $(j = (1,\ ...,\ M))$ are defined in (6). We remark that the Lie derivatives quantify the impact of changes in the control input (u_i) on the output function (h). Additionally, we denote with $dL^k_{f_{i_1},...,f_{i_k}}h$, the gradient of the corresponding Lie derivative (i.e. $dL^k_{f_{i_1},...,f_{i_k}}h \equiv \nabla_S L^k_{f_{i_1},...,f_{i_k}}h$), and, we denote with $d\Omega$, the space spanned by all these gradients.

In this notation, the observability rank criterion can be expressed in the following way: *The dimension of the largest WLO sub-system at a given S_0 is equal to the dimension of $d\Omega$.*

We remark that the dimension of $d\Omega$, must be computed by considering the Lie derivatives along all the vector fields f_{i_j}. By only considering a part of these vector fields (or linear combinations of these vector fields), it is possible to obtain a dimension which is smaller than the one of the actual largest WLO sub-system. In mobile robotics, this remark corresponds to the well known property that the observability of a state, could need to consecutively move the robot along all the

directions allowed by its drive system. When only special controls are set (i.e. when the robot is constrained to move along special trajectories), the state observability could be lost. In this case it is fundamental to find the part of the original state which is observable, i.e. to perform a system decomposition for the considered trajectories.

We consider again the simple example introduced in section II, and we show that by using the observability rank criterion, we can answer the first question stated in the introduction. We obtain the same answer already provided in section II.

The computation of the rank for the system in (3) is straightforward. From the last equation in (3), we obtain: $L^0h = D$ whose gradient is $dL^0h \equiv w_1 = [1, 0, 0]$. The first order Lie derivatives are: $L^1_{f_1}h = \cos(\theta_R - \phi_R)$ and $L^1_{f_2}h = 0$. We have: $dL^1_{f_1}h \equiv w_2 = [0, \sin(\theta_R - \phi_R), -\sin(\theta_R - \phi_R)]$. It is easy to realize that each vector w_i obtained by extending the previous computation to every Lie derivative order, has the structure: $w_i = [\varrho_i, \varsigma_i, -\varsigma_i]$. Indeed, every Lie derivative will depend on θ_R and ϕ_R only through the quantity $\theta_R - \phi_R$, whose sign changes with respect to the change $\theta_R \leftrightarrow \phi_R$. Therefore, the rank of the matrix

$$\Gamma \equiv \left\{ w_1^T,\ w_2^T,\ ...,\ w_i^T,\ ... \right\} \tag{8}$$

is equal to two. We conclude that the largest WLO subsystem, has dimension two as derived in section II.

B. Local Decomposition

Let us suppose that the system in (6) is not WLO and that the dimension of the largest WLO subsystem is n_{obs}. According to the theory of distributions developed in [17], we can find n_{obs} independent functions of the components of the original state S, which are WLO and $n - n_{obs}$ independent functions of the components of S, which are not WLO. More precisely, if we include the n_{obs} WLO functions in the vector S_b, and the other $n - n_{obs}$ functions in the vector S_a, we have the following decomposition for the original system:

$$\left\{ \dot{S}_a = \sum_{i=1}^{M} f_i^a(S_a, S_b)u_i, \quad \dot{S}_b = \sum_{i=1}^{M} f_i^b(S_b)u_i, \quad y = h_b(S_b) \right. \tag{9}$$

In particular, the subsystem defined by the last two equations in (9), is independent of the value of S_a and it is WLO. Therefore, by performing this decomposition, we can use the information coming from the dynamics (i.e. the knowledge of $u(t)$) and the observations ($y(t)$) in order to estimate the observable modes (S_b). This decomposition extends the Kalman canonical decomposition to the non linear case. It is fundamental in every estimation problem when the state is not observable. Indeed, estimating the original state S directly, results in an erroneous evaluation.

In section II, the equations in (5) represent such a decomposition for the system defined by (1-2) or (3).

C. Continuous Symmetries

We refer to the input-output system given in (6). We start by remarking that all the available information that we want to use to estimate the state S, is contained in the sensor data during a given time interval; specifically in the proprioceptive data (used to evaluate the system inputs u) and the exteroceptive data (used to evaluate the system outputs y). On the other hand, the knowledge of the system inputs and outputs in a given time interval, is equivalent to the knowledge of all the Lie derivatives at the initial time of the considered interval. This equivalence is the basis of the theory introduced by Hermann and Krener in [15] and, it is a consequence of the two theorems of the implicit functions and of the Taylor expansion. Hence, the points in the configuration space where all the Lie derivatives have the same values, cannot be distinguished by using the system inputs and outputs collected during a given time interval. For this reason, it is fundamental to determine the regions in the configuration space where all the Lie derivatives are invariant. We call them *indistinguishable regions*. Let us consider the state S_0 in the configuration space. Intuitively speaking, we call *continuous symmetry* in S_0, a continuous transformation which allows us to determine the associated indistinguishable region (i.e. the region where all the Lie derivatives have the same values as they have in S_0)

In the following, we provide a mathematical definition of indistinguishable region and our definition of continuous symmetry respectively. Then, we provide the procedure to determine the indistinguishable regions associated to the continuous symmetries. Finally, we derive theoretical results which play a key role to detect the observable modes for a given input-output system. We address the reader to [22] for additional results.

We introduce the following definition:

Definition 1 (Indistinguishable Region) *Given a system described by (6), an indistinguishable region associated to a point $S_0 \in \Sigma$ is a connected set in Σ, which contains S_0 and the points where all the Lie derivatives have the same value as in S_0.*

As previously mentioned, the points in the configuration space where all the Lie derivatives have the same values, cannot be distinguished by using the system inputs and outputs collected during a given time interval. This is the reason why we call these sets, indistinguishable regions.

Definition 2 (Continuous Symmetry) *The vector field $w_s(S)$ ($S \in \Sigma$), is a continuous symmetry in S for the system defined in (6), if and only if, it is a non-null vector belonging to the null space of the matrix, whose lines are the gradients of all the Lie derivatives computed in S. Mathematically: $\nabla_S L^k_{f_{i_1},...,f_{i_k}} h(S).w_s(S) = 0,\ \forall k,\ i_1,\ ...,\ i_k$.*

We now provide the procedure to build an indistinguishable region associated to a given continuous symmetry. Let us consider a point $S_0 \in \Sigma$ and the curve $S(S_0,\ \tau)$ in Σ, which is the solution of the differential equation:

$$\left\{ \frac{dS}{d\tau} = w_s(S), \qquad S(0) = S_0 \right. \tag{10}$$

(we assume suitable regularity hypotheses on $w_s(S)$, in order to guarantee the existence of a unique solution).

We prove that the curve $S(S_0,\ \tau)$, is an indistinguishable region of S_0. Before proving this, we prove the following property:

Property 1 *A scalar and differentiable function $g(S)$ ($S \in \Sigma$) is constant on the curve $S(S_0, \tau)$, if and only if, its gradient is orthogonal to $w_s(S)$.*

Proof: Proving this property is immediate. We have: $\frac{dg(S(S_0,\ \tau))}{d\tau} = \nabla_S g\ .\ \frac{dS}{d\tau} = \nabla_S g\ .\ w_s$ ■

Property 2 *The curve $S(S_0,\ \tau)$, which is the solution of equation (10), is an indistinguishable region of S_0.*

Proof: According to the definition 2, w_s is orthogonal to the gradients of all the Lie derivatives. From property 1 we obtain that all the Lie derivatives are constant on the curve $S(S_0,\ \tau)$ ■

It is immediate to extend this result by considering the following differential equation, which generalizes the equation in (10) when the system has N_s symmetries ($w_s^1,\ w_s^2,\ ...,\ w_s^{N_s}$):

$$\begin{cases} \dfrac{dS}{d\tau} &= \displaystyle\sum_{i=1}^{N_s} w_s^i(S)\eta_i(\tau), \qquad S(0) \quad = S_0 \end{cases}$$

for every choice of the functions $\eta_1(\tau),\ ...,\ \eta_{N_s}(\tau)$ (provided that the chosen functions guarantee a unique solution for the previous differential equation). The equation in (10), corresponds to the case when all the $\eta_i(\tau)$ are identically 0 with the exception of one of them, which is equal to 1.

To better illustrate the previous concepts, we discuss again the simple example provided in section II. For the system defined in (3), only one continuous symmetry given by the vector $[0,\ 1,\ 1]^T$ exists (i.e. belonging to the null space of the matrix Γ in (8)). Let us provide an intuitive interpretation of this continuous symmetry. It is possible to see that this symmetry corresponds to a rotation, which is a global symmetry (independent of S). Indeed, by denoting with $S_0 = [D_0,\ \phi_0,\ \theta_0]^T$, the curve $S(S_0, \tau)$, i.e. the solution of (10), is in this case:

$$\left\{ D(\tau) = D_0, \quad \phi(\tau) = \phi_0 + \tau, \quad \theta(\tau) = \theta_0 + \tau \right.$$

In other words, the continuous transformation defining this indistinguishable region, is the one performing the change $D_0 \rightarrow D_0$, $\phi_0 \rightarrow \phi_0 + \tau$ and $\theta_0 \rightarrow \theta_0 + \tau$ where τ is the continuous parameter characterizing the transformation. On the other hand, the previous transformation corresponds to a rotation of an angle τ. Therefore, this analytical result expresses what we already expected. Indeed, both the outputs and the inputs for the system in (3), are invariant with respect to a global rotation (see fig. 1).

We now provide the main result in order to deal with real systems, and to have an analytical procedure to determine its observable modes. We have the following property:

Property 3 *The gradient of any observable mode ($g(S)$) is orthogonal to $w_s(S)$ (i.e. $\nabla_S g\ .\ w_s(S) = 0$).*

Proof: We proceed by contradiction. Suppose that $\exists\ S_0$ such that $\nabla_S g|_{S_0}\ .\ w_s(S_0) \neq 0$. From the Taylor theorem we have: $g(S(S_0,\ \tau)) = g(S_0) + \nabla_S g|_{S_0}\ .\ w_s(S_0)\ \tau\ +\ o(\tau^2)$. Hence, $\exists\ \tau_M > 0$ such that $\forall\ \tau \in (0,\ \tau_M]$, $g(S(S_0,\ \tau)) \neq g(S_0)$. Since $g(S)$ is an observable mode, the points $S(S_0,\ \tau)$, $\tau \in (0,\ \tau_M]$, can be distinguished from S_0. This last sentence contradicts the result of property 2 ■

The previous condition can be expressed by the following partial differential equation:

$$\sum_{i=1}^{n} w_{si}(S)\frac{\partial g}{\partial S_i} = 0 \tag{11}$$

where $w_{si}(S)$ is the i^{th} component of the symmetry w_s. In other words, for every symmetry there is an associated partial differential equation which must be satisfied by all the observable modes.

We conclude this section by considering the example in section II. In particular, we use (11) to detect the two observable modes. As previously mentioned, this system has only the symmetry $[0,\ 1,\ 1]^T$. Hence, the associated equation (11) becomes: $\frac{\partial g}{\partial \phi_R} + \frac{\partial g}{\partial \theta_R} = 0$ and two independent solutions are $g = D$ and $g = \theta_R - \phi_R$. This is the same result we obtained in section II.

It is fundamental to remark, that for this simple example the corresponding symmetry has a very clear physical meaning, being a global rotation. As a result, the corresponding observable modes also have a clear physical meaning, being the quantities invariant under this rotation (not surprisingly they are distance and angle). On the other hand, the definition 2 is very abstract. Hence, there are cases where it is totally impossible to find a physical meaning for the symmetries of a given system, and consequently for its observable modes. In these cases, no intuitive method for derivation of observable modes exists and application of the proposed approach is necessary. This will be the case for the calibration problem analyzed in the next sections.

IV. The Problem of Simultaneous Odometry and Bearing Sensor Calibration

In contrast to the simple example introduced in section II, where a simple intuitive procedure provides the answers to the theoretical questions stated in the introduction, there are cases where the application of the previous concepts and in particular the use of (11), is required.

Here, we discuss a calibration problem. In this case, the proposed method autonomously derives the observable modes whose physical meaning cannot be found.

A. The Considered System

Again we consider a mobile robot moving in a $2D$-environment whose dynamics are described by (1). Now we assume that the odometry sensors do not provide directly v and ω. We will consider the case of a differential drive, and in order to characterize the systematic odometry errors, we adopt the model introduced in [7]. We have:

$$v = \frac{r_R\omega_R + r_L\omega_L}{2} \qquad \omega = \frac{r_R\omega_R - r_L\omega_L}{B} \tag{12}$$

where ω_R and ω_L are the control velocities (i.e. $u = [\omega_R,\ \omega_L]^T$) for the right and left wheel, B is the distance between the robot wheels and r_R and r_L are respectively the radius of the right and left wheel.

A bearing sensor (e.g. a camera) is mounted on the robot. We assume that its vertical axis is aligned with the $z-$axis of the robot reference frame, and therefore, the transformation between the frame attached to this sensor and the one of the robot, is characterized through the three parameters ϕ, ρ and ψ (see fig. 2).

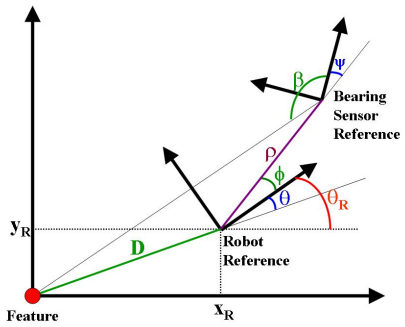

Fig. 2. The two reference frames respectively attached to the robot and to the bearing sensor.

The available data are the control $u = [\omega_R, \omega_L]^T$ and the bearing angle of a single feature (β in fig. 2) at several time steps during the robot motion. We introduce the following quantities:

$$\mu \equiv \frac{\rho}{D}; \quad \gamma \equiv \theta + \phi; \tag{13}$$

By using trigonometry algebra we obtain (see also fig. 2):

$$\beta = \begin{cases} -\arctan\left(\dfrac{\sin\gamma}{\mu+\cos\gamma}\right) - \psi + \pi & if\ \gamma_- \le \gamma \le \gamma_+ \\ -\arctan\left(\dfrac{\sin\gamma}{\mu+\cos\gamma}\right) - \psi & otherwise \end{cases}$$

where γ_- and γ_+ are the two solutions (in $[-\pi, \pi)$) of the equation $\cos\gamma = -\mu$ with $\gamma_+ = -\gamma_-$ and $\gamma_+ > 0$. We make the assumption $0 < \mu < 1$ as we want to avoid collisions between the robot and the feature ($D > \rho$).

By using (1) and the definitions in (13), the dynamics of our system are described by the following equations:

$$\begin{cases} \dot\mu = -\mu^2 \dfrac{v}{\rho}\cos(\gamma - \phi) \\ \dot\gamma = \omega - \mu\dfrac{v}{\rho}\sin(\gamma - \phi) \\ \dot\phi = \dot\rho = \dot\psi = \dot r_R = \dot r_L = \dot B = 0 \end{cases} \tag{14}$$

The goal is to simultaneously estimate the parameters ϕ, ρ, ψ, r_R, r_L and B, by using the available data (i.e. ω_R, ω_L and β in a given time interval). Since these data consist of angle measurements, the best we can hope is the possibility to estimate these parameters up to a scale factor. In other words, the estimation of the four parameters ρ, r_R, r_L and B, requires metric information which is not provided by the sensor data. Mathematically, this is a consequence of the fact that we can express both the dynamics and the observation in terms of the following parameters:

$$\phi, \qquad \psi, \qquad \eta \equiv \frac{r_R}{2\rho}, \qquad \delta \equiv \frac{r_L}{r_R}, \qquad \xi \equiv \frac{r_R}{B} \tag{15}$$

which are the original angle parameters and suitable ratios of the original parameters, which contain metric information (i.e. ρ, r_R, r_L and B). From now on, we will refer to the parameters in (15). However, at the end of section V, we show that by adding a simple metric measurement (e.g. the initial distance between the robot and the feature), the original parameters ϕ, ρ, ψ, r_R, r_L and B, can also be estimated.

By using the new parameters in (15), we obtain the following expressions for the dynamics and the observation:

$$\begin{cases} \dot\mu = -\mu^2\eta(\omega_R + \delta\omega_L)\cos(\gamma - \phi) \\ \dot\gamma = \xi(\omega_R - \delta\omega_L) - \mu\eta(\omega_R + \delta\omega_L)\sin(\gamma - \phi) \\ \dot\phi = \dot\psi = \dot\eta = \dot\delta = \dot\xi = 0 \\ \beta = \begin{bmatrix} -\arctan\left(\dfrac{\sin\gamma}{\mu+\cos\gamma}\right) - \psi + \pi & \gamma_- \le \gamma \le \gamma_+ \\ -\arctan\left(\dfrac{\sin\gamma}{\mu+\cos\gamma}\right) - \psi & otherwise \end{bmatrix} \end{cases} \tag{16}$$

The state $[\mu,\ \gamma,\ \phi,\ \psi,\ \eta,\ \delta,\ \xi]^T$ is WLO as proven in appendix A. Note that, to achieve the full observability, the robot must move along all the allowed degrees of freedom (i.e. all the inputs ω_R and ω_L must be considered). In the next subsection we consider circular trajectories (i.e. trajectories characterized by a constant ratio $\frac{\omega_R}{\omega_L}$). For them, the overall system is not WLO. We separate the part of the system which is WLO from the rest by using the theory introduced in section III-C. Based on this decomposition, in section V we introduce a very efficient strategy to estimate these parameters. This strategy is based on a closed-form solution which has been derived for circular trajectories. This solution allows a deterministic method (described in section V-A) to be introduced, which can then be used to initialize a method based on a Maximum A Posteriori (MAP) scheme or, more simply, based on a Least Squares (LS) scheme. When the robot controller is not precise enough to follow a circular path with good accuracy, the MAP scheme can be directly applied to the system defined in (16). In this case, the initial state estimated is: $[\mu_0,\ \gamma_0,\ \phi,\ \psi,\ \eta, \delta, \xi]$. Section V-B describes a simple least squares approach, which estimates the initial state observable when the robot accomplishes circular trajectories.

For the sake of clarity, we report all the variables adopted in the considered calibration problem in table I.

B. Deriving the Observable Modes for Circular Trajectories

We consider the motion obtained by setting

$$\omega_R = \nu; \qquad \omega_L = q\nu \tag{17}$$

Original Calibration Parameters Camera: $\phi,\ \rho,\ \psi$ Odometry: $r_R,\ r_L,\ B$
Observable Parameters $\phi, \quad \psi, \quad \eta \equiv \frac{r_R}{2\rho}, \quad \delta \equiv \frac{r_L}{r_R}, \quad \xi \equiv \frac{r_R}{B}$
Parameters observable in a single q-trajectory $A^q \equiv \frac{\Psi_1^q - \Psi_3}{1+\Psi_1^q\Psi_3}, V^q \equiv \Psi_2^q \frac{1+\Psi_1^q\Psi_3}{1+\Psi_3^2},$ $L^q \equiv \psi - \arctan\Psi_1^q, \xi_q \equiv \xi(1-q\delta)$ where: $\Psi_1^q \equiv \frac{\xi_q - \eta_q \sin\phi}{\eta_q \cos\phi}, \quad \Psi_2^q \equiv \frac{\mu\eta_q\cos\phi}{\sin\gamma},$ $\Psi_3 \equiv \frac{\mu+\cos\gamma}{\sin\gamma}, \quad \eta_q \equiv \eta(1+q\delta)$

TABLE I
VARIABLES ADOPTED IN OUR CALIBRATION PROBLEM

being q, a time-independent parameter. The corresponding trajectory is a circumference whose radius is: $\frac{B}{2}\frac{r_R+qr_L}{r_R-qr_L}$. In this section we focus our attention on a single value of q.

We remark that circular trajectories play a fundamental role in wheeled robotics. For a wheeled vehicle to exhibit rolling motion, a point must exist around which each wheel of the vehicle follows a circular course [33]. This point is known as Instantaneous Center of Rotation (ICR) and can be computed by intersecting all the roll axes of the wheels. For cars, the existence of the ICR is ensured by the Ackermann steering principle [33]. This principle ensures a smooth movement of the vehicle, by applying different steering angles to the inner and outer front wheel while turning. This is necessary, as all the four wheels move in a circle on four different radii around the ICR. Hence, the observable modes here derived, are also the observable modes for a generic trajectory but during very short intervals of time. Also, note that these trajectories have recently been used in the framework of aerial navigation [11].

By substituting (17) in (16) we obtain a new system, characterized by the same state as in (16), but with a single input (ν) instead of two (ω_R and ω_L). As a result, the weak local observability of the entire state $[\mu,\ \gamma,\ \phi,\ \psi,\ \eta,\ \delta,\ \xi]^T$ is lost: this is proven in appendix B where we prove that the system is not even weakly observable[1]. We therefore wonder, which are the observable modes for the new system.

Intuitively speaking, we must reduce the number of variables to describe our system (i.e. the observation and the dynamics), as in the example discussed in section II where we reduced the dimension from three to two. The system in (16) is described by seven variables/parameters. It is easy to reduce this number to six by introducing the two parameters:

$$\eta_q \equiv \eta(1+q\delta) \qquad \xi_q \equiv \xi(1-q\delta) \tag{18}$$

Indeed, both the observation and the dynamics in (16) can be expressed in terms of $[\mu,\ \gamma,\ \phi,\ \psi,\ \eta_q,\ \xi_q]^T$. In particular, the observation only depends on μ, γ and ψ, and the dynamics become:

$$\begin{cases} \dot{\mu} &= -\mu^2\eta_q\nu\cos(\gamma-\phi) \\ \dot{\gamma} &= \xi_q\nu - \mu\eta_q\nu\sin(\gamma-\phi) \\ \dot{\eta}_q = \dot{\xi}_q &= \dot{\phi} = \dot{\psi} = 0 \end{cases} \tag{19}$$

[1]We remind the reader that a system which is not weakly observable, is certainly not weakly locally observable (WLO); we address the reader to [15] for the definitions of *weak observability* and *weak local observability*

At this point we wonder if it is possible to further decompose this system (i.e. to further reduce the number of variables/parameters in order to describe the same system). In answer to this question, it is necessary to apply the rank criterion, i.e. we need to compute the dimension of the linear space containing the gradients of all the Lie derivatives of the system, with the dynamics in (19) and the observation in (16). In the case where this rank is equal to 6 (which is the dimension of the vector $[\mu,\ \gamma,\ \phi,\ \psi,\ \eta_q,\ \xi_q]^T$) in at least one point of the space of the states, we cannot proceed with the decomposition. In appendix C, we prove that this rank is smaller than 6 in every point of the states' space.
In order to further decompose this system, we need to adopt the method illustrated in section III. As we will see, the method is able to autonomously introduce new quantities whose physical meaning cannot be found. Finding a physical meaning for the quantities automatically introduced by the proposed method, is equivalent to finding an alternative, and probably easier procedure able to solve the same problem.

In the following, we provide the steps necessary to perform this decomposition. We first consider the simpler system:

$$\begin{cases} \dot{\mu} &= -\mu^2\eta_q\nu\cos(\gamma-\phi) \\ \dot{\gamma} &= \xi_q\nu - \mu\eta_q\nu\sin(\gamma-\phi) \\ \dot{\eta}_q = \dot{\xi}_q &= \dot{\phi} = 0, \quad y = \dfrac{\sin\gamma}{\mu+\cos\gamma} \end{cases} \tag{20}$$

where we removed the variable ψ. The state $[\mu,\ \gamma,\ \phi,\ \eta_q,\ \xi_q]^T$ $5-$dimensional. On the other hand, the dimension of the linear space containing the gradients of all the Lie derivatives of the system with the dynamics in (20), and the observation in (16), is smaller than 5 (the proof follows the same steps as the proof given in appendix C). By using the matlab symbolic computation, it is possible to detect the following symmetry:

$$w_s = \left[\mu\cos\gamma+1,\ \ \sin\gamma,\ \ \frac{\xi_q\sin\phi-\eta_q}{\mu},\ 0,\ \ \frac{\xi_q\cos\phi}{\eta_q\mu}\right]^T$$

Since this subsystem is defined by a $5-$dimensional state, having one symmetry means that we have four independent observable modes, which must satisfy the partial differential equation given in (11) associated to the previous symmetry:

$$(\mu\cos\gamma+1)\frac{\partial\Psi}{\partial\mu}+\sin\gamma\frac{\partial\Psi}{\partial\gamma}+\frac{\xi_q\sin\phi-\eta_q}{\mu}\frac{\partial\Psi}{\partial\eta_q}+\frac{\xi_q\cos\phi}{\eta_q\mu}\frac{\partial\Psi}{\partial\phi}=0$$

Finding four independent solutions is not difficult since we know that all the Lie derivatives are solutions. However, we need to express the dynamics and the system output using only these solutions, as in the decomposition given in (9). Therefore, we cannot simply use the Lie derivatives, since their expression is very complicated (with the exception of the zero-order which coincides with the output $\frac{\sin\gamma}{\mu+\cos\gamma}$). On the other hand, a very simple solution for the previous partial differential equation is provided by ξ_q. By using this solution and the output $\frac{\sin\gamma}{\mu+\cos\gamma}$, and starting from the expressions of the first and second order Lie derivatives, we were able to detect two other solutions: $\frac{\xi_q-\eta_q\sin\phi}{\eta_q\cos\phi}$ and $\frac{\mu\eta_q\cos\phi}{\sin\gamma}$. We therefore find the following four independent observable modes:

$$\Psi_1^q \equiv \frac{\xi_q - \eta_q \sin\phi}{\eta_q \cos\phi},\ \ \Psi_2^q \equiv \frac{\mu\eta_q \cos\phi}{\sin\gamma},\ \ \Psi_3 \equiv \frac{\mu + \cos\gamma}{\sin\gamma},\ \ \xi_q \tag{21}$$

and the local decomposition of (20) is:

$$\begin{cases} \dot{\Psi}_2^q = \nu\Psi_2^q(\Psi_1^q\Psi_2^q - \xi_q\Psi_3) \\ \dot{\Psi}_3 = \nu(\Psi_2^q + \Psi_1^q\Psi_2^q\Psi_3 - \xi_q - \xi_q\Psi_3^2) \\ \dot{\xi}_q = 0, \quad \dot{\Psi}_1^q = 0, \quad y = \dfrac{1}{\Psi_3} \end{cases} \tag{22}$$

We now add the parameter ψ (with $\dot{\psi} = 0$) to the system in (22) and we consider the output $y = \beta = \arctan\left(\frac{1}{\Psi_3}\right) - \psi$ instead of $y = \frac{1}{\Psi_3}$. In other words, we consider our original system described by the new 5-dimensional state $[\Psi_1^q,\ \Psi_2^q,\ \Psi_3,\ \xi_q,\ \psi]^T$, which is smaller than the dimension of the state $[\mu,\ \gamma,\ \phi,\ \psi,\ \eta_q,\ \xi_q]^T$. Again we ask if we can further proceed with the decomposition. In answer to this question it is necessary to apply the rank criterion to the system satisfying the dynamics in (22), and with the observation $y = \beta = \arctan\left(\frac{1}{\Psi_3}\right) - \psi$. It is possible to prove that the dimension of the linear space containing the gradients of all the Lie derivatives, is always smaller than 5 (which is the dimension of the vector $[\Psi_1^q,\ \Psi_2^q,\ \Psi_3,\ \xi_q,\ \psi]^T$): the proof is similar to the proof given in appendix C. Therefore, we re-apply the method from section III.

By using the matlab symbolic computation, it is possible to detect a single symmetry as in the system in (20):

$$w_s = \left[\Psi_1^{q^2} + 1,\ \Psi_2^q(\Psi_3 - \Psi_1^q)),\ \Psi_3^2 + 1,\ 0,\ 1\right]^T$$

Since this subsystem is defined by a $5-$dimensional state, having one symmetry means that we have four independent observable modes which must satisfy the partial differential equation given in (11) associated to the previous symmetry, i.e.:

$$(\Psi_1^{q^2}+1)\frac{\partial G}{\partial \Psi_1^q} + (\Psi_2^q(\Psi_3 - \Psi_1^q))\frac{\partial G}{\partial \Psi_2^q} + (\Psi_3^2+1)\frac{\partial G}{\partial \Psi_3} + \frac{\partial G}{\partial \psi} = 0$$

Namely, every solution $G(\Psi_1^q, \Psi_2^q, \Psi_3, \xi_q, \psi)$ of the previous partial differential equation, is a WLO quantity for the system in (22). Again, a very simple solution is provided by ξ_q. Then, by proceeding as before, we found the following four independent solutions:

$$A^q \equiv \frac{\Psi_1^q - \Psi_3}{1 + \Psi_1^q\Psi_3},\ V^q \equiv \Psi_2^q\frac{1 + \Psi_1^q\Psi_3}{1 + \Psi_3^2},\ L^q \equiv \psi - \arctan\Psi_1^q,\ \xi_q \tag{23}$$

and the local decomposition is:

$$\begin{cases} \dot{A}^q = \nu(1 + A^{q^2})(\xi_q - V^q) \\ \dot{V}^q = \nu A^q V^q(2V^q - \xi_q) \\ \dot{L}^q = \dot{\xi}_q = 0 \\ \beta = -\arctan(A^q) - L^q + S_p\dfrac{\pi}{2} \end{cases} \tag{24}$$

where S_p can be ± 1 depending on the values of the system parameters and the initial robot configuration. In section IV-C, we derive some important properties relating S_p to the robot motion. This decomposition has a very practical importance. It tells us that, when the robot accomplishes circular trajectories, the information contained in the sensor data (i.e. the information contained in the function $\nu(t)$ and $\beta(t)$), allows us to estimate only the state $[A^q,\ V^q,\ L^q,\ \xi_q]^T$ and not the original state $[\mu,\ \gamma,\ \phi,\ \psi,\ \xi,\ \delta,\ \eta]^T$. Furthermore, it provides the link between the observable state $[A^q,\ V^q,\ L^q,\ \xi_q]^T$ and the sensor data ν and β. By using the equations in (24), it would be possible to introduce an observer scheme to perform the estimation of the state $[A^q,\ V^q,\ L^q,\ \xi_q]^T$. On the other hand, because of the non linearity in both the dynamics and the observation, such an approach would be suboptimal. In the rest of this paper we will focus on the calibration problem, i.e. the estimation of the calibration parameters. Since in most cases, it is not important to perform the calibration on line, we will use the previous decomposition to introduce a calibration strategy based on a Least Squares (LS) scheme. Before introducing the strategy, we need to derive several analytical properties of the observation function.

C. Analytical Properties of the Observation Function

In this section, we summarize some important properties of the observation β obtained when the robot accomplishes circular trajectories. These properties are fundamental to introduce our calibration strategy. For the sake of conciseness, we cannot derive these properties here. However, a detailed derivation is available in [21]. Furthermore, it is possible to directly verify the validity of these properties with a simple substitution. For the sake of simplicity, in the following, we do not use the suffix q in the three parameters A, V and L. On the other hand, since ξ already exists, we maintain the q in ξ_q.

It is possible to directly integrate the dynamics in (24) to get an analytical expression for β vs the time, or vs the curve length s, defined by the following equation:

$$s = s(t) = \int_0^t \nu(\tau)d\tau \tag{25}$$

The expression of β vs s is given by the following equations (26-29). In particular, β depends on A (equation (29)), A depends on V (equation (28)), V depends on w (equation (27)) and finally w depends on s (equation (26)).

$$w = \xi_q \tan(c + S_w\xi_q s) \tag{26}$$

$$V = \frac{\xi_q k(2k - \xi_q) + kw^2 + S_V w\sqrt{k(k - \xi_q)(w^2 + \xi_q^2)}}{(2k - \xi_q)^2 + w^2} \tag{27}$$

$$A = S_y\sqrt{\frac{k(2V - \xi_q) - V^2}{V^2}} \tag{28}$$

$$\beta = \arctan(A) - L + S_p\frac{\pi}{2} \tag{29}$$

where S_w, S_V, and S_y are three sign variables, as S_p; they can assume the value of $+1$ or -1. c and k are two time-independent parameters, whose value depends on the initial robot configuration with respect to the feature. In particular:

$$k = \frac{(1+A_0^2)V_0^2}{2V_0 - \xi_q} \tag{30}$$

and

$$c = \arctan\left(\frac{\xi_q k + (\xi_q - 2k)V_0}{\xi_q\sqrt{-V_0^2 + 2kV_0 - \xi_q k}}\right) \tag{31}$$

The validity of the previous expression for β can be checked by directly computing the time derivatives of V and A in (27) and (28) respectively, and, by verifying that they satisfy (24).

It is a key advantage to have the analytical expression of the observation function $\beta(s)$. Indeed, since this expression depends on the calibration parameters, by experimentally collecting real data, we can estimate these parameters (e.g. with a least square fit, see section V-B). On the other hand, it is necessary to known how the sign variables depend on the curve length s in order to fit real data with the previous analytical expression. We remind the reader that the function $\beta(s)$ provides the bearing angle of the origin in the camera frame when the robot accomplishes circular trajectories. Since the circumference is an analytic curve, the function $\beta(s)$ must be C^∞ (with the exception of the discontinuity of 2π, artificially introduced to set the value of β in the interval $[-\pi,\ \pi)$). In the following, we derive the dependence of the sign variables on the curve length s by requiring continuity properties for the function $\beta(s)$ and its first derivative. From the expressions (26-29), we infer that the analysis can be restricted to the points where the function w in (26) diverges, and when the function V in (27) vanishes. We call the former points *nodes* and the latter *k-nodes*. Their expression is respectively:

$$s_n = -S_w\frac{c}{\xi_q} + j\frac{\pi}{\xi_q} + S_w\frac{\pi}{2\xi_q} \tag{32}$$

$$s_{kn} = -S_w\frac{c}{\xi_q} + j\frac{\pi}{\xi_q} - \frac{S_w S_V}{\xi_q}\arctan\left(\sqrt{-\frac{k}{\xi_q}}\right) \tag{33}$$

j being an integer. In other words, there are infinite nodes at the distance of $\frac{\pi}{|\xi_q|}$ from each other. The k-nodes exist if and only if, $-k\xi_q \geq 0$. In order to ensure the continuity of $\beta(s)$ and its first derivative, S_V and S_y must flip in correspondence to each node, and S_y and S_p must flip in correspondence to each k-node (see [21] for the details).

We also consider the point where the function $w(s)$ in (26) vanishes. We call them *mirror points*. Their expression is:

$$s_{mp} = -S_w\frac{c}{\xi_q} + j\frac{\pi}{\xi_q} \tag{34}$$

for every integer j. From (32) and (33) we have: $s_n = s_{mp} + S_w\frac{\pi}{2\xi_q}$ and $s_{kn} = s_{mp} - \frac{S_w S_V}{\xi_q}\arctan\left(\sqrt{-\frac{k}{\xi_q}}\right)$.

In Fig 3 we represent all the previous points. Fig 3a refers to the case when the k-nodes do not exist ($k\xi_q > 0$). We assumed $S_w = 1$, and for the sake of clarity, we assumed $S_V = S_y = S_p = 1$ on the right of the first indicated node. In both cases, we observe that S_V, S_y and S_p all have the same value when s of $2\frac{\pi}{|\xi_q|}$ is increased. Since $\frac{2\pi}{|\xi_q|}$ is a multiple of the period of w, this means that the observation function is a periodic function with period:

$$T_S = \frac{2\pi}{|\xi_q|} \tag{35}$$

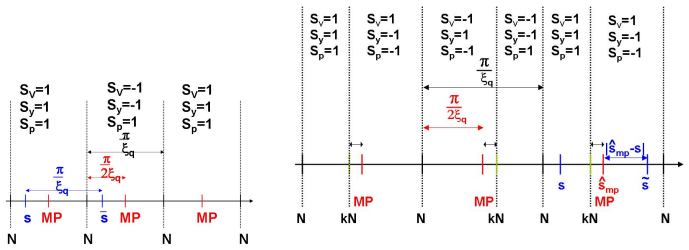

Fig. 3. Special points where the sign variables change their value. a illustrates the case when k-nodes do not exist and b when they do exist.

Finally, we introduce two operations. Let us consider a generic point s. The former is called *shift* and associates s with the value $\overline{s} \equiv s + \frac{T_S}{2}$. The latter is called *reflection*. We denote with s_{mp}^R the closest mirror point to s on the right. The reflection associates s with the point $\widetilde{s}$ which is the symmetric point of s with respect to s_{mp}^R (see fig 3a for an illustration). From this definition we have $s + \widetilde{s} = 2s_{mp}^R$, i.e.: $\widetilde{s} \equiv 2s_{mp}^R - s$.

It is easy to verify that the operations of shift and reflection are commutative. We will indicate with $\hat{s}$, the point obtained when these two operations are both applied to s (i.e. $\hat{s} \equiv \widetilde{\overline{s}}$). By indicating with s_n^R the closest node to s on the right, it results that $\hat{s}$ is the symmetric point of s with respect to s_n^R (see fig 3a for an illustration), namely:

$$\hat{s} = 2s_n^R - s \tag{36}$$

In [21] we derive the following fundamental theorem whose validity can in any case be checked by a direct substitution:

Theorem 1 (Reflection and shift of the observation) *The observation function satisfies the following fundamental equation* $\forall s$*:*

$$\beta(s) + \beta(\hat{s}) = -2L\ (\mod \pi) \tag{37}$$

where $\mod$ *is the remainder of a division.*

Proof: The proof of this theorem is provided in [21] ■

This theorem is fundamental to estimate the parameters ξ_q, L, k and c for a given trajectory (see the algorithm 1 in the next section). The name reflection comes from the fact that, according to (36), $\hat{s}$ is the reflection of s with respect to the node (s_n^R) in between them.

The previous theorem is basically a consequence of the circular trajectory accomplished by the robot. However, in [21] its proof is carried out by performing a continuity analysis on the observation function. The advantage of this analysis is that it provides the behavior of the sign variables (S_V, S_y and S_p).

V. The Strategy to Estimate the System Parameters

The results obtained in the previous section, allow us to introduce a non-iterative method in order to estimate the observable state $[\xi_q,\ L,\ c,\ k]^T$. We will call this the *deterministic method* and we will denote it with DET. It will be described in V-A. The performance of DET can be further improved by minimizing a specific cost function. We will denote with LS the method which minimizes this cost function (section V-B). Finally, in V-C we provide a method to estimate the calibration parameters starting from the values of ξ_q and L for three distinct trajectories.

A. The deterministic method

The first step of DET consists in estimating ξ_q by evaluating the period of the observation function, and then by using (35). In fact, this equation does not provide the sign of ξ_q. However, this sign is positive for all the values of $q < \frac{1}{\delta}$ (i.e. when the robot accomplishes counter clock-wise circular trajectories). Once ξ_q is estimated, the next step consists of the evaluation of the position of one node. The algorithm 1, describes the procedure to perform this evaluation. It computes the left hand side of equation (37), called $\theta(s_c, s)$, for every possible node candidate (s_c), which is in the interval $[0, \frac{T_S}{2}]$. The function $\theta(s_c, s)$, is independent of the second argument s when $s_c = s_n$. Indeed, $\theta(s_n, s) = -2L\ \forall s$. This means that the standard deviation of $\theta(s_c, s)$ with respect to the second argument (s), is zero when computed in s_n (i.e. $\sigma(s_n) = 0$). When the robot sensors are affected by measurement errors, the function $\sigma(s_c)$ attains its minimum in s_n (see figures 6*c*, 6*d*, 7*c* and 7*d*.

Algorithm 1 (Returns one Node)
for s_c = *0 to* $\frac{T_S}{2}$ ***do***
  for s = *0 to* $\frac{T_S}{2}$ ***do***
    $\hat{s} = 2s_c - s$
    $\theta(s_c, s) = \beta(s) + \beta(\hat{s})(\mod \pi)$
  end for
end for
for s_c = *0 to* $\frac{T_S}{2}$ ***do***
  $\sigma(s_c)$ = *standard deviation of* $\theta(s_c, s)$
end for
$s_n = \arg\min_{s_c} \sigma(s_c)$

Once s_n is determined, equations (36) and (37) allow us to immediately evaluate the parameter L. Additionally, equation (32) allows us to evaluate c. In both cases, few possible values for these parameters are actually provided. The correct ones can be selected by combining more than one circular trajectory. The value of k can be estimated from the following expression:

$$k = \frac{\xi_q}{1 - \tan^2\left(\frac{\beta(m_1) - \beta(m_2)}{2}\right)} \tag{38}$$

where m_1 and m_2 are the positions of two consecutive mirror points (see [21] for the derivation of the previous equation). Fig. 4 displays the steps of the deterministic method.

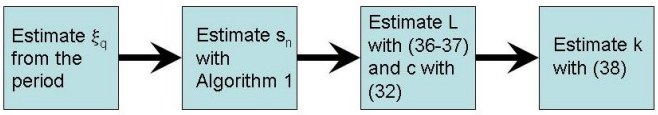

Fig. 4. The steps performed by the deterministic method.

B. A simple least squares approach

Let us suppose that the camera performs N bearing observations, and let us indicate these values with β_i^{obs} ($i = 1, ..., N$). Also, let us indicate the corresponding values of the curve length with s_i. s_i are provided by the odometry sensors. In the absence of measurement errors, $\beta_i^{obs} = \beta(s_i)$, β being the function defined in (26-29). Since the expression of β depends on the parameters ξ_q, L, c and k, their value can be obtained by minimizing the cost function: $\sum_{i=1}^{N} \frac{\left(\beta_i^{obs} - \beta(s_i)\right)^2}{\sigma_i^2}$, where σ_i weights the terms in the sum, according to the measurement errors (it increases with the curve length because of the odometry drift). In section VI, we minimize the previous cost function by using the Levenberg Marquadt algorithm, and, by adopting the DET method for the initialization.

C. Estimation of the Calibration Parameters

Once the parameters ξ_q and L are estimated for at least three independent trajectories (i.e. corresponding to three different values of q, q_1, q_2 and q_3), the calibration parameters ϕ, ψ, η, δ and ξ, can be found by using (18), the first equation in (21) and the last equation in (23). In particular, by having the value of ξ_q for two trajectories, it is possible to get the parameters ξ and δ by using the second equation in (18). Then, by using (18) and the first in (21), we obtain the following equation:

$$\eta_x \Psi_1^q + \eta_y = f_q$$

where $\eta_x \equiv \eta \cos\phi$, $\eta_y \equiv \eta \sin\phi$ and $f_q \equiv \xi \frac{1 - q\delta}{1 + q\delta}$. By using two distinct trajectories (corresponding to q_1 and q_2), we can solve the linear system

$$\begin{bmatrix} \Psi_1^{q_1} & 1 \\ \Psi_1^{q_2} & 1 \end{bmatrix} \begin{bmatrix} \eta_x \\ \eta_y \end{bmatrix} = \begin{bmatrix} f_{q_1} \\ f_{q_2} \end{bmatrix}$$

where $\Psi_1^q = \tan(\psi - L^q)$. In this way, we obtain both η_x and η_y in terms of ψ. By using the third equation $\eta_x \Psi_1^{q_3} + \eta_y = f_{q_3}$, we can compute ψ.

As mentioned in section IV-A, the information provided by the sensor data only allows us to estimate the parameters ϕ, ψ, η, δ and ξ, i.e. the calibration parameters up to a scale factor. However, by adding a supplementary metric measurement, we can also estimate the original parameters ϕ, ρ, ψ, r_R, r_L and B. Let us suppose that we know the initial distance of the robot from the feature for one of the three trajectories, and, that it is the trajectory defined by $q = q_1$. Once the parameters ϕ, ψ, η, δ and ξ are estimated as previously explained, we also consider the parameters c and k for the trajectory with $q = q_1$. By using (30) and (31), we obtain the values of A_0 and V_0. Then, by using the first two equations in (23), we obtain the corresponding Ψ_2^q and Ψ_3^q at $s = 0$. From the last

r	K	ν
$0.3m$	$0.001m^{\frac{1}{2}}$	$0.168\ rad\ s^{-1}$

TABLE II
PARAMETERS CHARACTERIZING THE ODOMETRY SYSTEM.

ϕ	ρ	ψ	r_R	r_L	B
$0.0000deg$	$0.30000m$	$90.000deg$	$0.297m$	$0.3018m$	$0.485m$

TABLE III
THE CALIBRATION PARAMETERS ADOPTED IN OUR SIMULATIONS

two equations in (21), we obtain the initial values γ_0 and μ_0. On the other hand, knowing the initial distance D_0, allows us to obtain $\rho = \mu_0 D_0$. Once ρ is evaluated, we can estimate $r_R = 2\rho\eta$ and then $r_L = \delta r_R$ and $B = \frac{r_R}{\xi}$.

VI. PERFORMANCE EVALUATION

We evaluate the performance of the proposed calibration strategy by carrying out both simulations and experiments. Since in the simulations the ground truth is available, we compare our strategy with a method based on an Extended Kalman Filter (EKF). This method uses an EKF to integrate the encoders data with the data provided by the camera. The equations of this filter are obtained from the standard EKF equations (e.g. see [4]), whose ingredients are provided in appendix D. From now on, we will refer to this calibration method as $CEKF$ (Calibration based on the EKF).

A. Simulations

The dynamics of the simulated robot are described by the equations (1) and (12). The robot is equipped with encoder sensors which provide the rotations of the right and the left wheel occurring at every time step. These encoder data are delivered at $50Hz$. Additionally, according to the model introduced in [10], all these measurements are affected by zero mean Gaussian errors, independent of each other. In particular, according to the error model in [10], the variance of each measurement is proportional to the value provided by the sensor. In other words, let us suppose that the true rotations of the right and left wheel which occur at a given time step, are equal to $\delta\alpha_R^{true}$ and $\delta\alpha_L^{true}$. We generate the following measurements: $\delta\alpha^{R/L} = N\left(\delta\alpha_{R/L}^{true}, \frac{K_{R/L}^2}{r_{R/L}^n}|\delta\alpha_{R/L}^{true}|\right)$, where $N(m,\sigma^2)$ indicates the normal distribution with mean value m and variance σ^2. r_R^n and r_L^n are the nominal values of the radius of the right and left wheel, and K_R and K_L characterize the non systematic odometry error. We have considered many different values for the parameters characterizing the simulated odometry system (i.e. K_R, K_L, r_R^n, r_L^n, the robot speed and the distance between the wheels (B)). Our strategy was always precise, even when we considered values of K_R and K_L much larger (roughly a hundred times) than the values obtained through real experiments (see [10] where $K_R \simeq K_L \simeq 5\ 10^{-4} m^{\frac{1}{2}}$).

In this section we provide a part of the results obtained from our simulations. We set $r \equiv r_R^n = r_L^n$ and $K \equiv K_R = K_L$. In table II, we report the characteristics of the robot dynamics. Note that, the chosen K was larger than the experimental values provided in [10], i.e. we simulated less accurate encoder sensors which was more challenging for our strategy.

The simulated exteroceptive sensor provided the bearings of a single feature at the origin. These data were delivered at $1Hz$. We assumed that these bearing measurements were affected by a zero mean Gaussian error. In other words, we generated the following measurement: $\beta = N(\beta^{true}, \sigma_\beta^2)$, where β^{true} was the true bearing of the feature in the local frame of the sensor. We performed many simulations by varying the value of σ_β in the range $[0,5]deg$.

Finally, we considered many values for the calibration parameters: ϕ, ρ, ψ, r_R, r_L and B. However, the performance of our strategy does not depend on them. For this reason, we show a single case. Table III provides the values of the calibration parameters adopted in the simulations.

Figure 5 reports the results obtained from the ideal case where both the odometry and the bearing sensor were noiseless (i.e. $\sigma_\beta = K = 0$). We show two cases. In the first, the observed feature was inside the accomplished trajectory and in the second, it was outside. The motion was characterized by $q = 0.8$ (the values of the other parameters have previously been specified). The robot trajectories and the feature are displayed in figure $5a$ and $5b$. Figure $5c$ shows the observation function with the two nodes (red stars) for the motion shown in figure $5a$, and figure $5e$ shows the function $\sigma(s_c)$. s_c is the supposed position of one node. When s_c is equal to the true node position, the function $\sigma(s_c)$ attains its minimum. In this case, the minimum is equal to zero since it refers to an ideal case. Figures $5d$ and $5f$ refer to the case shown in figure $5b$.

Figure 6 displays the results obtained by setting $\sigma_\beta = 1deg$ and the value of K as specified in table II. In this case, we performed three trajectories corresponding to three different values of q: 0.9, 0 and -1. In figure 6 we only display the results related to $q = 0.9$ (figures $6a$, $6c$ and $6e$) and $q = -1$ (figures $6b$, $6d$ and $6f$). In particular, figures $6a$ and $6b$ display the observation functions with the nodes (red stars), figures $6c$ and $6d$ display the functions $\sigma(s_c)$ and figures $6e$ and $6f$ display the observation functions as observed (blue points) estimated by DET (red points) and improved with LS (black points). We remarked that the difference between the red and the black line, is actually due to a poor estimation of the parameter k. Indeed, DET only uses two observations to estimate k (see equation (38)).

Figure 7 displays the same results as shown in figure 6, but with a noisier bearing sensor ($\sigma_\beta = 5deg$). In this case, the minimum of $\sigma(s_c)$ is significantly larger than 0 (figures $7c$ and $7d$).

By combining the estimated ξ_q and L for the three considered robot trajectories (i.e. with $q = 0.9,\ 0,\ -1$), we finally estimate the five parameters ϕ, ψ, η, δ and ξ. In table IV, we provide the values obtained for different errors on the bearing sensor (i.e. $\sigma_\beta = 1,\ 3,\ 5\ deg$). These results are obtained by using DET for the initialization and then by using LS. The number of exteroceptive observations is 300. Even with a large error on the bearing sensor($\sigma_\beta = 5deg$), it is

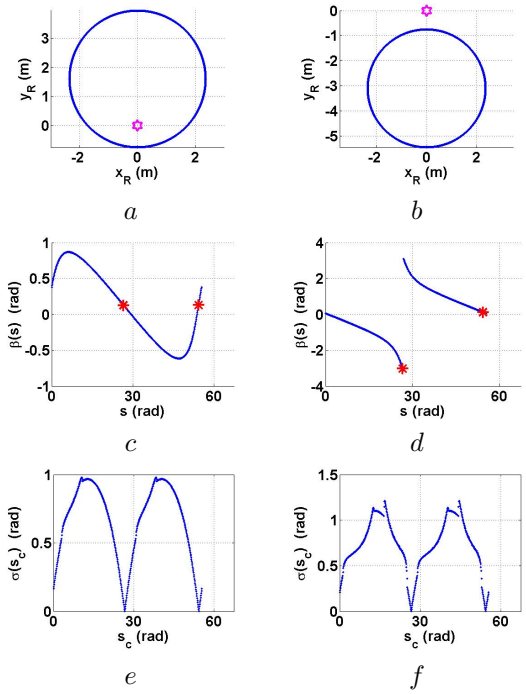

Fig. 5. The nodes detection phase from our strategy for the ideal case of perfect sensors when $q = 0.8$. a, c and e refer to the case when the feature is inside the accomplished trajectory, while b, d and f, when it is outside . a and b display the trajectories, c and d display the observation functions with the estimated nodes and e and f display the functions $\sigma(s_c)$.

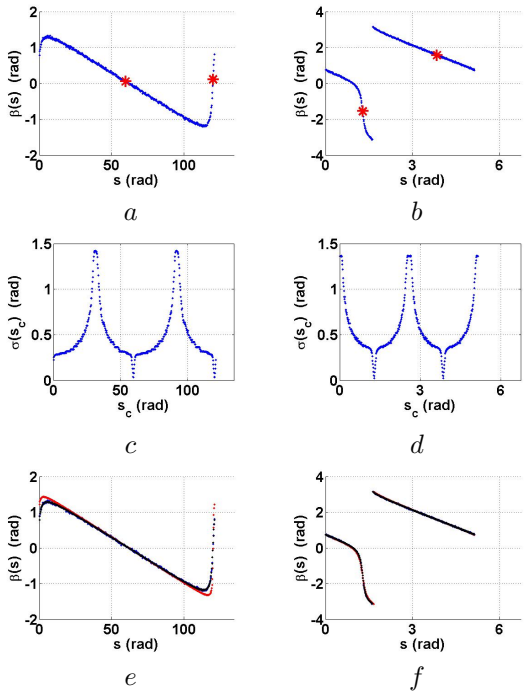

Fig. 6. The estimation of the nodes and of the parameters ξ_q, L, c and k when $q = 0.9$ (a, c and e), and $q = -1$ (b, d and f). $\sigma_\beta = 1deg$ and $K = 0.001m^{\frac{1}{2}}$. a and b display the observation functions with the estimated nodes, c and d display the functions $\sigma(s_c)$, and e and f display the observation functions as observed (blue dots), estimated by DET (red dots) and improved by LS (black dots).

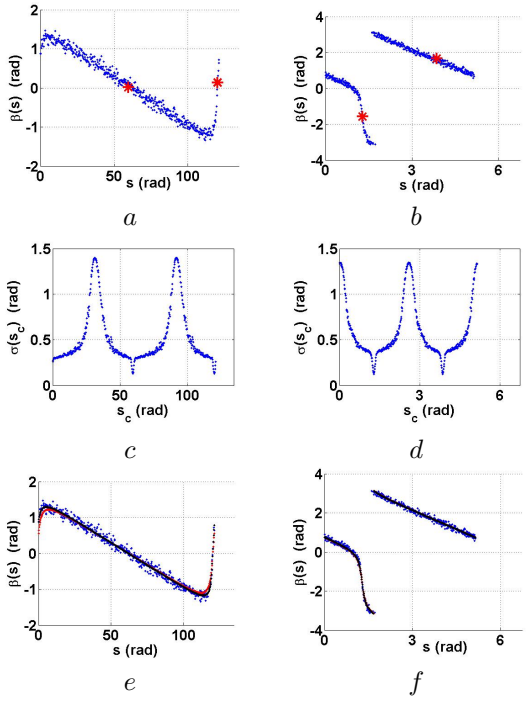

Fig. 7. As in figure 6 but with a larger error on β ($\sigma_\beta = 5deg$).

σ_β	ϕ (deg)	ψ (deg)	η	δ	ξ
True	0.00	90.0	0.49500	1.01616	0.61236
$1deg$	-0.08	90.05	0.49596	1.01610	0.61296
$3deg$	0.21	90.08	0.49362	1.01629	0.61167
$5deg$	0.13	89.83	0.50103	1.01607	0.61323

TABLE IV
THE VALUES OF THE CALIBRATION PARAMETERS ADOPTED IN OUR SIMULATION. TRUE VALUES (FIRST LINE) AND VALUES OBTAINED BY LS (INITIALIZED WITH DET) FOR DIFFERENT σ_β.

possible to achieve a high level of accuracy. In particular, on the parameter δ the relative error is smaller than 0.01% when $\sigma_\beta = 1deg$. We also remark that in our simulation, the robot accomplishes the circular trajectory only once. It is possible to further improve the accuracy by moving the robot along more than one loop for every q, and/or, by considering more than three values of q. Table IV refers to a single simulation. In order to have a more indicative result, we performed 100 complete simulations, obtaining 100 values for every estimated parameter. We compute the error of the estimated parameters for every simulation. In table V, we report the mean value for these errors. The parameter $\imath$ describes how the trajectory satisfies the circular hypothesis (see next paragraph). It is possible to see that the relative error on the estimated parameters is small.

1) Checking the ideal hypothesis of circular path: We investigate the impact of a path which is not perfectly circular. To this goal, we divide the circular path in ten thousand segments. For each one we compute the corresponding displacement for the right and left wheel (Δs_R^c and Δs_L^c). Then, we randomly generate the displacements of both of these wheels (Δs_R and Δs_L) with a Gaussian distribution: $\Delta s_R = N(\Delta s_R^c, (\imath \times \Delta s_R^c)^2)$ and $\Delta s_L = N(\Delta s_L^c, (\imath \times \Delta s_L^c)^2)$. We

$\imath$	σ_β deg	$\Delta\phi$ deg	$\Delta\psi$ deg	$\frac{\Delta\eta}{\eta}$ %	$\frac{\Delta\delta}{\delta}$ %	$\frac{\Delta\xi}{\xi}$ %
0.0	1	0.10	0.08	0.32	0.005	0.045
0.02	1	0.65	0.37	1.5	0.05	0.15
0.04	1	1.3	0.5	3.2	0.10	0.19
0.0	3	0.19	0.13	0.53	0.012	0.087
0.02	3	1.2	0.71	2.5	0.11	0.25
0.04	3	2.2	0.9	5.2	0.23	0.41
0.0	5	0.28	0.23	0.85	0.019	0.13
0.02	5	1.7	1.0	3.9	0.18	0.56
0.04	5	3.1	1.6	5.7	0.35	0.66

TABLE V
THE ERRORS ON THE ESTIMATED PARAMETERS AVERAGED ON 100 SIMULATIONS FOR THREE DIFFERENT σ_β AND THREE DIFFERENT $\imath$.

consider three cases: $\imath = 0$ (i.e. perfect circular trajectory), $\imath = 0.02$ and $\imath = 0.04$. In fig. 8, we plot the ratio $\frac{\Delta s_L}{\Delta s_R}$ vs time when the robot accomplishes a circular trajectory characterized by $q = 0.7$. On the left, the real case obtained by using the robot AMV-1[1] from the BlueBotics company is displayed, and on the right we display the ratio for the simulated robot when $\imath = 0.02$. We realize that the real case satisfies the circular hypothesis better than the case when $\imath = 0.02$. Table V shows the effect of $\imath$ on the estimation process. The results refer to the case where the number of bearing observations is 100.

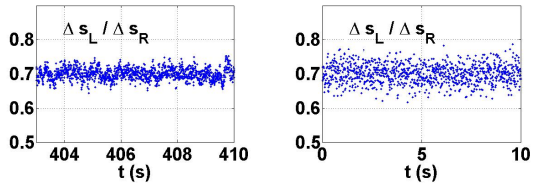

Fig. 8. The ratio $\frac{\Delta s_L}{\Delta s_R}$ vs time when the robot accomplishes a circular trajectory ($q = 0.7$). On the left, the result obtained with the real robot AMV-1 and on the right, our simulated robot when $\imath = 0.02$.

2) Comparison with CEKF: As previously mentioned, we have also adopted an EKF to estimate the observable modes for a given trajectory. In contrast to the deterministic method, it is necessary for this filter to initialize the parameters. We obtained that in order to have the convergence, the initial relative error must not exceed 40%, and regarding L, the initial error must be smaller than $30deg$. Table VI shows the performance of $CEKF$, DET and LS. The errors of the parameters are averaged on 100 simulations. $CEKF_d$ differs from $CEKF$ since, in the former, the initialization is performed by using DET. In $CEKF$, the relative error on the initial state is equal to 30%. It is possible to remark that LS always outperforms the other methods.

3) The effect of systematic errors: Because of imperfect wheel encoders/controller, when the robot is commanded to execute a trajectory with a given q, it actually accomplishes a trajectory characterized by $q + \delta q$. We performed simulations by considering different values of δq (for all three values of q requested by the proposed strategy). The results are shown in table VII.

[1]See [1] for a description of the robot

$Method$	$\imath$	σ_β deg	$\frac{\Delta\xi_q}{\xi_q}$ %	ΔL deg	Δc deg	$\frac{\Delta k}{k}$ %
$CEKF$	0.04	5	9.3	4.3		
	0	5	2.8	1.5		
	0.04	1	5.8	3.5		
	0	1	1.7	0.75		
DET	0.04	5	3.2	3.8	1.1	27
	0	5	1.4	1.1	0.45	16
	0.04	1	3.1	0.25	0.28	6.3
	0	1	1.5	0.061	0.093	2.7
$CEKF_d$	0.04	5	1.6	1.2		
	0	5	0.55	0.37		
	0.04	1	0.87	0.13		
	0	1	0.11	0.039		
LS	0.04	5	0.74	0.41	0.83	1.6
	0	5	0.23	0.17	0.22	0.85
	0.04	1	0.18	0.11	0.27	0.29
	0	1	0.059	0.040	0.065	0.12

TABLE VI
THE ERRORS OF THE PARAMETERS AVERAGED ON 100 SIMULATIONS ESTIMATED BY ALL THE METHODS HERE DISCUSSED.

δq	$\Delta\phi$ deg	$\Delta\psi$ deg	$\frac{\Delta\eta}{\eta}$ %	$\frac{\Delta\delta}{\delta}$ %	$\frac{\Delta\xi}{\xi}$ %
0.00	0.10	0.08	0.32	0.005	0.045
0.01	0.17	0.20	1.4	0.69	0.40
0.03	0.48	0.51	3.3	2.3	1.2
0.05	0.83	0.92	6.3	4.1	2.0
0.10	1.5	1.6	13	7.9	4.2

TABLE VII
THE ERRORS AVERAGED ON 100 SIMULATIONS FOR SEVERAL δq.

B. Real Experiments

To evaluate the performance of our strategy in a real case, we used the mobile robot e-puck[2]. In our experiments, we only used the camera and the odometry sensors. In fact, our strategy has been developed to calibrate an omnidirectional bearing sensor. In contrast, the available camera has a very limited angle of view ($\simeq 38deg$). In practice, it is generally not possible to observe a single feature during the entire circular trajectory accomplished by the robot. The only situation where this is possible, occurs when the feature is inside the circular trajectory (as represented in figure 5a) and close to the center. Additionally, the camera must look towards the center of the circumference. This is the case when the angle ϕ is close to $0deg$ and ψ is close to $90deg$. Since the available camera looks ahead, we fixed a small mirror onto the front of the robot (see figure 9a). Obviously, in these conditions, our strategy cannot estimate the extrinsic calibration parameters related to the real camera. However, it estimates the parameters of the virtual camera, i.e. the mirrored one. We remark that the goal of this experiment, is not to estimate the configuration of the true camera, but to validate our strategy. Therefore, it is not important whether the camera we are considering, is the real camera or not.

The robot camera provides images with resolution 60×60. Figure 9b is an image of the feature (consisting of a source of light) taken by the e-puck camera during our experiments. The images were provided at a frequency in the range $[0.5, 8]Hz$.

[2]See [13] for a detailed description of this robot and its sensors

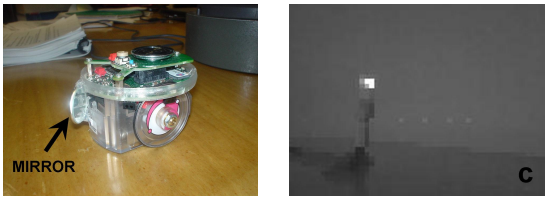

a b

Fig. 9. The robot e-puck with a small mirror in front of the camera (a) and, the feature observed by the robot camera (b).

We performed three complete experiments. In the last two, we increased the radius of the right and left wheel by $0.062mm$ using a piece of tape. Each experiment consisted of four independent trajectories with the following values, q: $0.9,\ 0.7,\ 0.6,\ 0.4$. In figure 10, we show the results of the parameters ξ_q, L, c and k, related to the case $q = 0.6$ without tape, and, the case $q = 0.4$ with tape on the left wheel. In both cases we show the observation function with the estimated nodes (10 a, and c) and the observation functions as observed (blue points), estimated by DET (red points) and improved with LS (black points) (10 b and d).

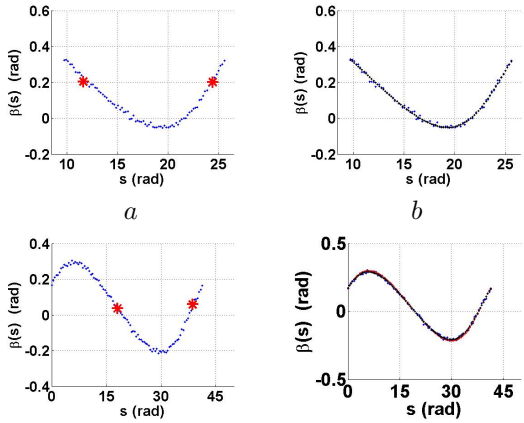

a b c d

Fig. 10. The estimation of the nodes and then the parameters ξ_q, L, c and k for the robot e-puck without tape and $q = 0.6$, and, $q = 0.4$ with tape on the left wheel. a and c display the observation function with the estimated nodes, b and d display the observation function as observed (blue points), estimated by DET (red points) and improved with LS (black points).

Table VIII reports the values of the parameters ξ_q, L, c and k, obtained in our experiments for the different trajectories (i.e. the four considered values of q) in the three considered cases. From these values, we obtained the calibration parameters for the three cases reported in table IX. Regarding the angles ϕ and ψ, we remark that the difference among the three cases is smaller than $0.3deg$. We believe that in our case, $\sigma_\beta \simeq 1deg$ and $0 < \imath < 0.02$. Hence, the difference $0.3deg$ is approximately the mean error obtained in our simulations (see the third and fourth column of table V). This is consistent with the fact that the tape does not affect these angle parameters. On the other hand, we remark an important difference for the parameters η and δ. Regarding η, the difference is $\simeq 2\%$, which is larger than the mean error obtained in our simulations (see the fifth column of table V). Regarding δ, the difference

q	ξ_q	$L\ (rad)$	$c\ (rad)$	k
	Without	Tape		
0.9	0.0384	1.8469	-1.4644	0.0389
0.7	0.1142	1.6382	-1.2599	0.1217
0.6	0.1519	1.5291	-1.1587	0.1616
0.4	0.2287	1.3145	$-.9850$	0.2322
	Tape	on the	Right	Wheel
0.9	0.0393	1.8435	-1.4703	0.0401
0.7	0.1145	1.6355	-1.2845	0.1229
0.6	0.1531	1.5279	-1.1457	0.1627
0.4	0.2282	1.3103	-0.9737	0.2319
	Tape	on the	Left	Wheel
0.9	0.0368	1.8487	-1.4755	0.0378
0.7	0.1132	1.6402	-1.2703	0.1206
0.6	0.1511	1.5301	-1.1602	0.1609
0.4	0.2271	1.3167	-0.9359	0.2283

TABLE VIII
THE VALUES OF ξ_q, L, c AND k OBTAINED IN OUR EXPERIMENTS FOR THE CONSIDERED TRAJECTORIES.

Tape	$\phi\ (deg)$	$\psi\ (deg)$	η	δ	ξ
No	-5.80	117.18	0.2042	0.9987	0.3798
Right	-5.67	116.91	0.2080	0.9959	0.3794
Left	-5.73	117.10	0.2052	1.0027	0.3790

TABLE IX
THE CALIBRATION PARAMETERS ESTIMATED IN OUR EXPERIMENTS.

is $\simeq 0.7\%$, which is significantly larger than the mean error obtained in our simulations (see the sixth column of table V). This is consistent with the increased radius of the right wheel. In particular, since the wheel radius is $\simeq 2cm$, we obtain $\simeq 0.06mm$ for the radius change. The variation in the parameter ξ, is very small. In particular, it is $\simeq 0.1\%$ which is approximately the mean error obtained in our simulations (see the last column of table V). This parameter should be affected by the tape, since it depends on r_R. A possible explanation could be that the tape also increased the effective distance between the wheels (i.e. the parameter B), making $\xi = \frac{r_R}{B}$ almost unaffected by the tape on the right wheel, and decreasing, with the tape on the left wheel.

VII. CONCLUSION

In this paper, we considered the problem of estimation in autonomous navigation from a theoretical perspective. In particular, the investigation regarded problems where the information provided by the sensor data, was not sufficient to carry out the state estimation (i.e. the state was not observable). In order to properly exploit the information in the sensor data, it was necessary to separate the observable part of the system from the rest. We introduced the concept of continuous symmetry to achieve this goal. We illustrated this concept by providing a very simple example, where a global rotational symmetry was evident. In this case, we remarked that the observable modes were the quantities which were rotation invariant (specifically, one distance and one angle). Motivated by this result, we introduced a definition of continuous symmetry which generalizes the intuitive idea of symmetry. This allowed us to introduce a mathematical method which can be applied to derive the observable modes for more complex

systems. Continuous symmetry defines transformation, and, as for the simple case of rotation, the observable modes are the invariant quantities under this transformation. Since the proposed definition of continuous symmetry is totally abstract (it is a mathematical generalization of an intuitive concept), the corresponding transformation does not necessarily have a physical meaning. Consequently, the observable modes also do not necessarily have a physical meaning. This is a fundamental aspect of our approach. Indeed, the proposed method is able to autonomously derive the observable modes without necessarily knowing their physical meaning.

The concept of continuous symmetry was applied to investigate the observability properties of a calibration problem in wheeled robotics. It allowed us to introduce a non-iterative method to perform the calibration. In [22], [23], we proposed another application of continuous symmetry, which allowed us to analytically derive all the observable modes for the problem of fusing the data from a camera and inertial sensors.

We continue to consider other estimation problems, where the proposed concept of continuous symmetry could play a key role.

APPENDIX A
OBSERVABILITY FOR THE SYSTEM DEFINED BY EQUATION (16)

Let us refer to the system whose dynamics and observation are defined in (16). In order to prove that it is WLO, according to the rank criterion, we provide seven Lie derivatives whose gradients span the entire configuration space. Let us consider the matrix whose lines are the gradients of the Lie derivatives: $L^0\beta$, $L^1_{f_1}\beta$, $L^1_{f_2}\beta$, $L^2_{f_1f_1}\beta$, $L^2_{f_1f_2}\beta$, $L^2_{f_2f_1}\beta$ and $L^2_{f_2f_2}\beta$, where $f_1 = -\left[\mu^2\eta\cos(\gamma-\phi), \mu\eta\sin(\gamma-\phi)-\xi, 0, 0, 0, 0, 0\right]^T$ and $f_2 = -\delta\left[\mu^2\eta\cos(\gamma-\phi), \mu\eta\sin(\gamma-\phi)+\xi, 0, 0, 0, 0, 0\right]^T$. The determinant of this matrix is: $-16\delta^4\mu^5\eta^3\xi^5\cos(\gamma-\phi)(\mu\cos\phi-\cos(\gamma-\phi))/(\mu^2+2\mu\cos\gamma+1)^5$, which is different from 0 with the exception of the points where one of the following conditions is satisfied: $\mu\cos\phi=\cos(\gamma-\phi)$, $\gamma=\phi+j\frac{\pi}{2}$ (j being an integer). By indicating this set of points with Θ, we remark that its interior is empty (i.e. for every $S\in\Theta$, every open ball centered in S, contains at least one point outside Θ). Starting from this fact and by analyzing the dynamics in (16), it is possible to find a control able to move the state outside Θ instantaneously. For instance, by setting $\omega_L=-\omega_R$ and by remarking that $\delta\simeq 1$, we obtain from (16), $\dot{\mu}\simeq 0$ and $\dot{\gamma}\simeq 2\xi\omega_R$. Hence, both the equations defining Θ become unfulfilled.

APPENDIX B
NON WEAK OBSERVABILITY FOR THE SYSTEM DEFINED BY EQUATION (16) WITH THE CONSTRAINT ON ITS INPUT GIVEN IN (17)

Let us refer to the system whose dynamics and observation are defined in (16), when the single input is ν, according to the constraint given in (17). We will show that there are infinite initial states which cannot be distinguished.

Let us consider the initial state $S^0 \equiv [\mu^0,\ \gamma^0,\ \phi^0,\ \psi^0,\ \eta^0,\ \delta^0,\ \xi^0]^T$. All the initial states $S(\lambda)\equiv\left[\mu^0,\ \gamma^0,\ \phi^0,\ \psi^0,\ \frac{\eta^0(1+q\delta^0)}{1+q\lambda},\ \lambda,\ \frac{\xi^0(1-q\delta^0)}{1-q\lambda}\right]^T$ (being $\lambda\in\Re^+$) provide the same output (β) for any choice of the input ν. Indeed, the output in (16) only depends on μ, γ and ψ, whose dynamics are independent of λ. This proves the non-observability of the considered system. On the other hand, when $\lambda\to\delta^0$ $S(\lambda)\to S^0$. Hence, even states which are close to S_0 cannot be distinguished from S_0. Therefore, the system is not weakly observable according to the definition of weak observability given in [15].

APPENDIX C
OBSERVABILITY RANK CRITERION FOR THE SYSTEM WITH THE DYNAMICS IN (19) AND THE OBSERVATION IN (16)

According to the observability rank criterion, we need to calculate the dimension of the linear space containing the gradients of all the Lie derivatives of the observation function in (16) along the dynamics given in (19). On the other hand, since our system is affine in the input, we can restrict the computation to the first $n-1$ Lie derivatives, being n, the dimension of the state $[\mu,\ \gamma,\ \phi,\ \psi,\ \eta_q,\ \xi_q]^T$, i.e. $n=6$ and $n-1=5$ (see [2], chapter 4). By a direct computation carried out with the help of the matlab symbolic tool, we obtain that the determinant of the matrix whose lines are the gradients of the first five Lie derivatives and the observation function (which is the zero order Lie derivative), is equal to zero in every point of the space of the states. Therefore, the dimension of the linear space containing the gradients of all the Lie derivatives is always smaller than 6.

APPENDIX D
EKF-BASED APPROACH

Let us consider the state $[A,\ V,\ \xi_q,\ L]^T$, which contains all the observable modes when the robot accomplishes a circular trajectory. This state can be estimated with an EKF. On the other hand, we found more precise results by estimating the state $X\equiv[A_v,\ V,\ \xi_q,\ L]^T$, whose first component is $A_v\equiv AV$. Obviously X is still WLO. In the following, we provide the analytical expression for the Jacobians of the dynamics, and the observation to implement an EKF which estimates X. The dynamics of X are:

$$\begin{cases} \dot{A}_v = \nu(A_v^2 + V\xi_q - V^2) \\ \dot{V} = \nu A_v(2V^q - \xi_q) \\ \dot{L} = \dot{\xi}_q = 0 \\ \beta = -\arctan\left(\dfrac{A_v}{V}\right) - L + S_p\dfrac{\pi}{2} \end{cases} \tag{39}$$

The Jacobian of the observation is obtained by differentiating the expression of β with respect to X, i.e. $H\equiv\frac{\partial\beta}{\partial X}=\begin{bmatrix} -\frac{V}{V^2+A_v^2} & \frac{A_v}{V^2+A_v^2} & 0 & -1 \end{bmatrix}$. Regarding the Jacobian of the dynamics, we need first of all to discretize the equations in (39). Let us denote the curve length change occurred in a given time step with δs (i.e. $\delta s=\nu\delta t$, δt being the length of the considered step). The Jacobian of the dynamics with respect to the state X is:

$$F_x = \begin{bmatrix} 1+2\delta s A_v & \delta s(\xi_q - 2V) & \delta s V & 0 \\ \delta s(2V - \xi_q) & 1+2\delta s A_v & -\delta s A_v & 0 \\ 0 & 0 & 1 & 0 \\ 0 & 0 & 0 & 1 \end{bmatrix} \quad (40)$$

and with respect to the input (δs) is: $F_u = [A_v^2 + V\xi_q - V^2,\ A_v(2V - \xi_q),\ 0,\ 0]^T$.

ACKNOWLEDGMENT

This work was supported by the European Commission FP7-ICT-2007-3.2.2 Cognitive Systems, Interaction, and Robotics under the contract #231855 (sFLY). The author also wishes to thank Jean-Marc Bollon for the help provided with the experiment and Sarah Whittaker for editing the text.

REFERENCES

[1] http://www.bluebotics.com/automation/AMV-1/
[2] Anguelova M., Non linear Observability and Identifiability: General Theory and a Case Study of a Kinetic Model, PhD thesis, Goteborg, April 2004
[3] Antonelli G. and Chiaverini S., Linear estimation of the physical odometric parameters for differential-drive mobile robots, Autonomous Robot, Vol 23, pages 59–68
[4] Bar-Shalom Y., Tracking and data association, Academic Press Professional, Inc. San Diego, CA, USA, 1987
[5] Bicchi A., Pratichizzo D., Marigo A. and Balestrino A., On the Observability of Mobile Vehicles Localization, IEEE Mediterranean Conference on Control and Systems, 1998
[6] Bonnifait P. and Garcia G., Design and Experimental Validation of an Odometric and Goniometric Localization System for Outdoor Robot Vehicles, IEEE Transaction On Robotics and Automation, Vol 14, No 4, August 1998
[7] Borenstein J., Feng L., "Measurement and correction of systematic odometry errors in mobile robots," *IEEE Transactions on Robotics and Automation*, vol. 12, pp. 869–880, 1996.
[8] Brogan W. L. Modern Control Theory, 3rd ed. Englewood Cliffs, NJ: Prentice Hall, 1991
[9] Brun X. and Goulette F., Modeling and calibration of coupled fisheye CCD camera and laser range scanner for outdoor environment reconstruction, in Proceedings of the International Conference on 3D Digital Imaging and Modeling, Montreal, QC, Canada, Aug. 21-23, 2007, pp. 320-327.
[10] Chong K.S., Kleeman L., "Accurate Odometry and Error Modelling for a Mobile Robot," *International Conference on Robotics and Automation*, vol. 4, pp. 2783–2788, 1997.
[11] Cole D. T., Thompson P., Goktogan A. H., Sukkarieh S., "System Development and Demonstration of a Cooperative UAV Team for Mapping and Tracking", The International Journal of Robotics Research September 2010 vol. 29 no. 11 1371–1399.
[12] Doh N. L., Choset H. and Chung W. K., Relative localization using path odometry information, Autonomous Robots, Vol 21, pages 143–154
[13] http://www.e-puck.org/
[14] Goldstein, H. Classical Mechanics, 2nd ed. Reading, MA: Addison-Wesley, 1980
[15] Hermann R. and Krener A.J., 1977, Nonlinear Controllability and Observability, IEEE Transaction On Automatic Control, AC-22(5): 728–740
[16] Huang G.P., Mourikis A.I., and Roumeliotis S.I., "Analysis and improvement of the consistency of extended Kalman filter based Slam", In Proceedings of the 2008 IEEE International Conference on Robotics and Automation (ICRA), pages 473-479, May 2008.
[17] Isidori A., Nonlinear Control Systems, 3rd ed., Springer Verlag, 1995.
[18] Kosut R.L., Arbel A. and Kessler K.M., Optimal Sensor System Design for State Reconstruction, IEEE Transaction On Automatic Control, Vol 27, No 1, February 1982
[19] Lee K. W., Wijesoma W. S. and Guzman J.I., On the Observability and observability analysis of SLAM. In Proceedings of IEEE International Conference on Intelligent Robots and Systems, Benjing, China, October 2006.
[20] Lorussi F, Marigo A. and Bicchi A., Optimal exploratory paths for a mobile rover, IEEE International Conference on Robotics and Automation (ICRA), 2001, Vol 2, Pages: 2078–2083
[21] Martinelli A., Using the Distribution Theory to Simultaneously Calibrate the Sensors of a Mobile Robot, Internal Research Report, INRIA, http://hal.inria.fr/inria-00353079/en/
[22] Martinelli A., Continuous Symmetries and Observability Properties in Autonomous Navigation, Internal Research Report, INRIA, http://hal.archives-ouvertes.fr/inria-00421233/en/
[23] Martinelli A., Deriving and Estimating All the Observable Modes when Fusing Monocular Vision and Inertial Measurements: A Closed Form Solution. Transaction on Robotics (under review)
[24] Martinelli A., Scaramuzza D. and Siegwart R., Automatic Self-Calibration of a Vision System during Robot Motion, International Conference on Robotics and Automation, Orlando, Florida, April 2006.
[25] Martinelli A., Local Decomposition and Observability Properties for Automatic Calibration in Mobile Robotics, International Conference on Robotics and Automation, Kobe, Japan, May 2009.
[26] Martinelli A, Using the Distribution Theory to Simultaneously Calibrate the Sensors of a Mobile Robot, Robotics: Science and Systems, RSS 2009, Seattle, June 2009.
[27] Mirzaei F.M. and Roumeliotis S.I., A Kalman filter-based algorithm for IMU-camera calibration: Observability analysis and performance evaluation, IEEE Transactions on Robotics, 2008, Vol. 24, No. 5, October 2008, pages 1143–1156
[28] Park F.C. and Martin B.J., Robot Sensor Calibration: Solving AX=XB on the Euclidean Group, IEEE Trans. on Rob. and Aut., Vol 10, No 5 Oct 1994.
[29] Perera L., Wijesoma W.S. and Adams M., The Estimation Theoretic Sensor Bias Correction Problem in Map Aided Localization, International Journal of Robotics Research, Vol 25, Issue 7, July 2006.
[30] Roumeliotis S.I. and Bekey G.A., 2002, Distributed Multirobot Localization, IEEE Transaction On Robotics and Automation Vol 18, No.5, October 2002
[31] Roy N., and Thrun S., Online Self-calibration for Mobile Robots, proceedings of the 1999 IEEE International Conference on Robotics and Automation, 19 May 1999 Detroit, Michigan, pp. 2292–2297.
[32] Shiu Y.C. and Ahmad S., Calibration of Wrist-Mounted Robotic Sensors by Solving Homogeneous Transform Equations of the Form AX=XB, IEEE Trans on Rob. and Aut. Vol 5 No 1 Feb 1989
[33] Siegwart, R., Nourbakhsh, I.: Introduction to Autonomous Mobile Robots. MIT Press (2004)
[34] Von der Hardt H.J., Husson R., Wolf D., An Automatic Calibration Method for a Multisensor System: Application to a Mobile Robot Localization System, Interbational Conference on Robotics and Automation, Leuven, Belgium, May 1998.
[35] Wasielewski S. and Strauss O., Calibration of a multi-sensor system laser rangefinder/camera, in Proceedings of the Intelligent Vehicles Symposium, Detroit, MI, Sept. 25-26, 1995, pp. 472-477.
[36] Zhang Q. and Pless R., Extrinsic calibration of a camera and laser range finder (improves camera calibration), in Proceedings of the IEEE/RSJ International Conference on Intelligent Robots and Systems, Sendai, Japan, Sept. 28Oct. 2, 2004, pp. 2301-2306.

Agostino Martinelli Agostino Martinelli (1971) received the M.Sc. in theoretical Physics in 1994 from the University of Rome "Tor Vergata" and the PhD in Astrophysics in 1999 from the University of Rome "La Sapienza". During his PhD he spent one year at the University of Wales in Cardiff and one year in the School of Trieste (SISSA). His research was focused on the chemical and dynamical evolution in the elliptical galaxies, in the quasars and in the intergalactic medium. He also introduced models based on the General Relativity to explain the anisotropies on the Cosmic Background Radiation. After his PhD, his interests moved to the problem of autonomous navigation. He spent two years at the University of Rome "Tor Vergata" and, in 2002, he moved to the Autonomous Systems Lab, EPFL, in Lausanne as senior researcher, where he lead several projects on multi sensor fusion for robot localization, simultaneous localization and odometry error learning, and SLAM. Since September 2006 he is Researcher (CR1) at the INRIA Rhone Alpes in Grenoble. He has authored more than 50 journal and conference papers.